

Transient current responses of organic electrochemical transistors by vertical ionic diffusion and electrolyte resistance

Juan Bisquert*¹, Nir Tessler²

¹Instituto de Tecnología Química (Universitat Politècnica de València-Agència Estatal Consejo Superior de Investigaciones Científicas), Av. dels Tarongers, 46022, València, Spain.

²Andrew & Erna Viterbi Department of Electrical and Computer Engineering, Technion, Haifa 32000, Israel

2024 08 18

Corresponding author: jbisquer@itq.upv.es

Abstract

For the successful implementation of organic electrochemical transistors in neuromorphic computing, bioelectronics, and real-time sensing applications it is essential to understand the factors that influence device switching times. Here we describe a physical-electrochemical model of the transient response to a step of the gate voltage. The model incorporates (1) ion diffusion inside the channel that governs the electronic conductivity, (2) horizontal electron transport, and (3) the external elements (capacitance, ionic resistance) of the ion dynamics in the electrolyte. We find a general expression of two different time constants that determine the vertical insertion process in terms of the kinetic parameters, in addition to the electronic transit time. We thus obtain a generalization of Bernards-Malliaras model for the exponential transient, as well as a more general set of nonlinear equations that explain the large perturbation effects. The basic model is confirmed by detailed simulations that enable to visualize the different ions distributions and dynamics.

1. Introduction

Organic electrochemical transistors (OECTs) are presently under investigation for a variety of applications, including bioelectronics, logic circuit components, and neuromorphic devices.¹⁻⁷ In the OECT the channel is formed by a mixed ionic-electronic conductor.^{8,9} The variable electronic conductivity is obtained by insertion and extraction of ions from an electrolyte and subsequent ion diffusion in the channel, while the compensating electronic carriers are established from drain and source contacts.¹⁰⁻¹²

OECT are excellent for translating chemical signals, such as ions or neurotransmitters, into electrical signals, as well as for accurately controlling stable conductance states to efficiently emulate computational tasks performed by biological synapses such as short-term depression (STD), short term potentiation (STP), and long-term potentiation (LTP).¹³ However, fully capitalizing on OECTs requires a deeper comprehension of their fundamental transistor operation mechanisms, particularly regarding transistor switching behaviors, which play a pivotal role in the training phase of the neural networks. Controlling the device relaxation times is essential to increase the nonvolatility of neuromorphic transistor elements, by slowing down the ionic response, or inducing electrochemical reactions.

The switching properties have been investigated recently¹⁴⁻²⁴ and different conclusions have been obtained, regarding effects of the size of the cation, asymmetry of cation injection and extraction. The main approach to analyze the switching transient is the Bernardis-Malliaras (BM) model,² that captures the coupling of cation insertion and the compensating electronic charge, by combining the electronic transient time across the channel, τ_e , and the time τ_i , associated to series connection of the ionic resistance of the electrolyte and the gate. However, it is generally understood that the diffusion step of cations inside the channel is a dominant factor of the switching dynamics, and this was not included in BM. Recently, asymmetric switching times have been observed upon charging and discharging, and they have been interpreted as lateral diffusion currents along the channel.²⁴⁻²⁶

In our previous work, we developed a general transition line model of OECT considering drift electronic transport and ionic injection and diffusion across the organic film, driven by the gate voltage.²⁷ The derived analytical model describes the dependence of drain current on gate bias in a time-transient situation, according to the measurement outlined in Fig. 1a. However, experimental patterns are more complex, due to the influence of capacitive and resistive elements in the electrolyte and its interfaces to the gate and channel. As we have recently found the impedance expression of the general model,²⁸ including series impedances in the electrolyte, here we apply the theory of transients to show the types of decays that can be expected, their physical interpretation, and their evolution with the gate voltage.

2. Transients in the ion diffusion model

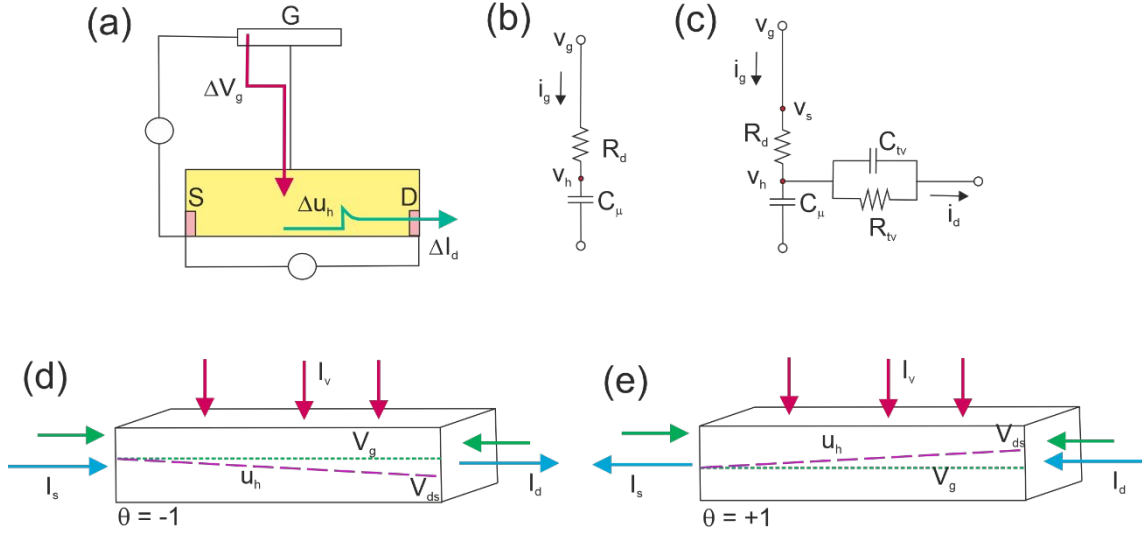


Fig. 1. (a) Scheme of the measurement of transient response of the OEET. (b) The equivalent circuit for the vertical small signal ac impedance. (c) The equivalent circuit for the transversal impedance. (d, e) The blue arrows indicate the stationary electronic current $I_d^{st} = I_s^{st}$. The green arrows are the transient charging electronic currents. In a transient situation, the difference of green currents at Drain and Source electrodes, $I_d - I_s$, equals the total ion current entering the channel film (red arrows). The voltage distribution for a small u_{ds} is indicated for two situations: (d) $\theta = -1, V_{ds} < 0$, and (e) $\theta = +1, V_{ds} > 0$.

2.1. General transport-conservation equations

We summarize the previous results for the transients measured in the configuration of Fig. 1a.²⁷ This model relies on a general transmission line approach, consisting on ionic diffusion from the electrolyte to fill the channel at the equilibrium concentration imposed by the gate voltage, combined with drift electronic transport across the channel, of charge injected from source and drain contacts, Fig. 1d, e. The following conventions are used for the voltages and currents. The variable voltages are denoted u_g (the gate voltage), u_d (the drain voltage); the voltages of the stationary point are denoted V_g, V_d, \dots , and finally, the small perturbation voltages are named v_g, v_d, \dots . The gate current is I_g , drain current is I_d , and the stationary currents are I_k^{st} . The I_d is positive in the x direction in Fig. 2a. Small perturbation currents are denoted i_k . The vertical small perturbation gate current is i_g and the drain current is i_d .

There are two kinetic constants, the electronic transit time, τ_e , and the vertical ion diffusion time, τ_d . These are defined by the expressions

$$\tau_e = \frac{L^2}{\mu_p |V_{ds}|} \quad (1)$$

$$\tau_d = \frac{d^2}{D_{ion}} \quad (2)$$

where L is channel length, μ_p is the hole mobility, V_{ds} is drain-source voltage, d is channel thickness, and D_{ion} is the ion diffusion coefficient inside the organic film. The direction

of electrical field in the channel is determined by the factor $\theta = V_{ds}/|V_{ds}|$, see Fig. 1d, e. Changing the sign of θ allows to turn the response of the drain into the corresponding response of the source current, which can also be measured.

Under certain conditions, related to homogeneous distribution of electronic and ionic carriers, the model for accumulation mode OECT can be reduced to the following two equations.²⁸ For the vertical current

$$I_g = C_\mu \frac{du_h}{dt} \quad (3)$$

$$I_g = -\frac{qL}{\tau_d} [A(u_g) - A(u_h)] \quad (4)$$

Here q is the elementary charge, I_g is the gate current, u_s is..., and A is the average concentration of anions per unit horizontal distance in the channel. The chemical capacitance is

$$C_\mu = -qL \frac{dA_{eq}}{du_g} \quad (5)$$

For the horizontal current we have

$$I_d = -\frac{q\theta L}{\tau_e} A - qL f_B \beta_\mu \frac{dA}{dt} \quad (6)$$

f_B is a symmetry factor, and the factor

$$\beta_\mu = \frac{1}{1 + \frac{A}{\mu_p} \frac{d\mu_p}{dA}} \quad (7)$$

is due to the density dependence of the mobility.²⁹ Note that it can be $\beta_\mu < 0$ if the mobility $d\mu_p/dA < 0$, which a common property.^{6,29,30}

Eq. (6) is already obtained in the BM model,¹⁵ and Eq. (4) is a simplified coupled diffusion equation.²⁷

2.2. The transient response to gate voltage step

Now we take an operating point V_g and we apply a small gate bias step perturbation ΔV

$$v_g = \Delta V H(t) \quad (8)$$

where $H(t)$ is the unit step function. For small perturbation voltages v_k and currents i_k .

Eq. (6) gives the stationary and time dependent equations:

$$I_d(t) = I_{d0}^{st} + i_d(t) \quad (9)$$

$$I_{d0}^{st} = -\frac{q\theta L}{\tau_e} A_{eq}(V_g) \quad (10)$$

$$i_d(t) = C_\mu \left[\frac{f_B \beta_\mu}{\tau_d} \Delta V + \left(\frac{\theta}{\beta_\mu \tau_e} - \frac{f_B \beta_\mu}{\tau_d} \right) v_h \right] \quad (11)$$

where

$$v_h = \Delta V (1 - e^{-t/\tau_d}) \quad (12)$$

We can write

$$i_d(t) = \left[\frac{f_B \beta \mu}{\tau_d} + \left(\frac{\theta}{\beta \mu \tau_e} - \frac{f_B \beta \mu}{\tau_d} \right) (1 - e^{-t/\tau_d}) \right] C_\mu \Delta V \quad (13)$$

Consider a concrete expression of the thermodynamic function²⁷

$$A_{eq}(u_g) = \frac{2}{3} A_0 \left[\frac{q(V_v - V_g)}{k_B T} \right]^{3/2} \quad (14)$$

with the corresponding chemical capacitance

$$C_\mu = -qL \frac{dA_{eq}}{d(V_g)} = \frac{A_0}{k_B T} \left[\frac{q(V_v - V_g)}{k_B T} \right]^{1/2} \quad (15)$$

The k_B is the Boltzmann's constant, T the absolute temperature, V_v the valence edge potential, A_0 a density per length.

Table 1

channel length	L	50 μm
thickness	d	100 nm
width	w	10 μm
Hole mobility	μ_p	0.02 cm^2/Vs
Source-drain voltage	$ V_{ds} $	0.1 V
Thermal energy	$k_B T$	0.026 V

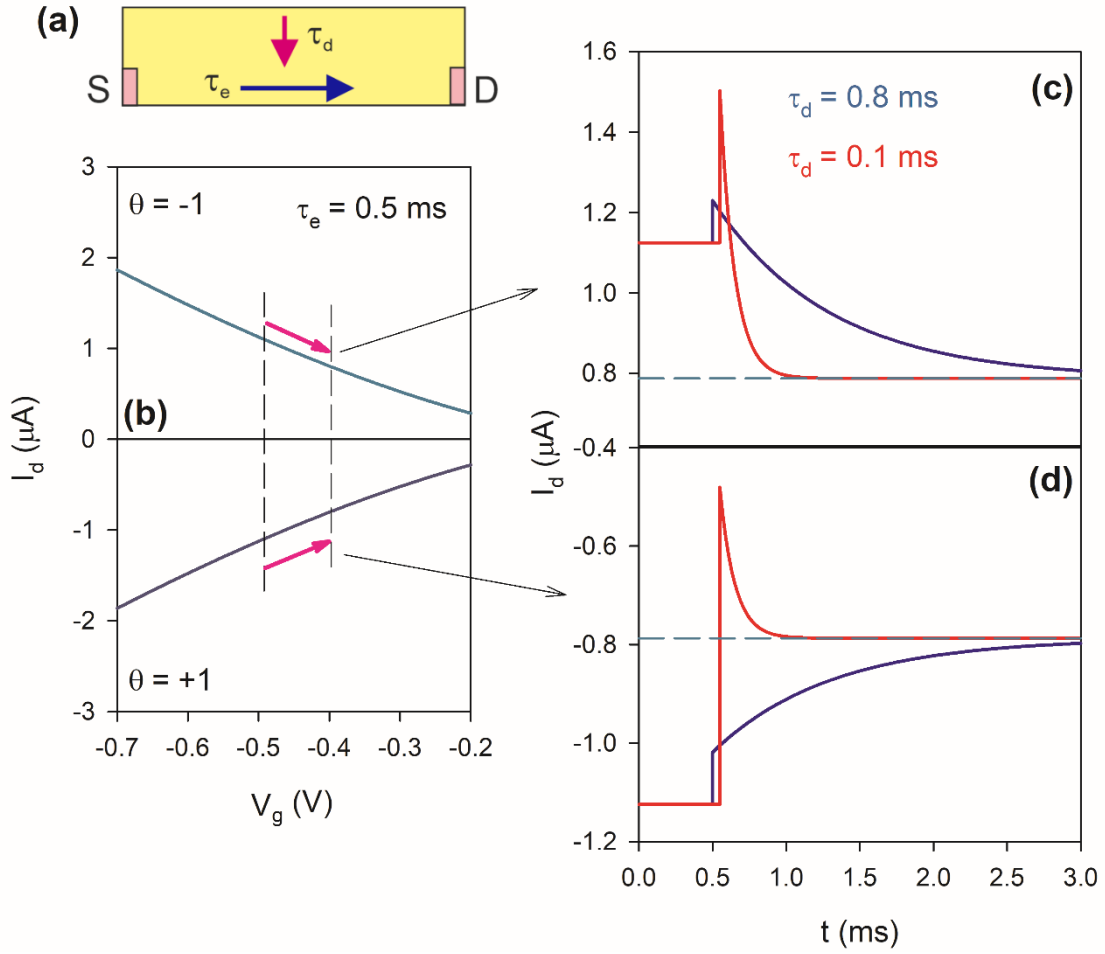


Fig. 2. (a) Scheme of the electrochemical transistor and the characteristic times processes. (b) The stationary current according to the sign $\theta = V_{ds}/|V|$ and (c, d) the possible four different types of transient response with respect to time, for a step voltage at $V_g = -0.5 \text{ V}$ and $\Delta V = 0.1 \text{ V}$ at $t_0 = 0.50, 0.51 \text{ ms}$. $A_0 = 6.2 \times 10^{12} \text{ m}^{-1}$, $V_v = 0$, $f_B = 0.5$, rest of parameters in Table 1.

Fig. 2 shows four current transient conditions, according to the sign of θ and the relative size of the dominant relaxation times τ_e and τ_d , by the parameters in Table 1.

The vertical diffusion resistance³¹ is

$$R_d = \frac{\tau_d}{c_\mu} \quad (16)$$

From Eq. (11), the initial current value is

$$i_{d0} = \frac{f_B \beta_\mu}{R_d} \Delta V \quad (17)$$

Therefore, the initial jump of the transient is a current through the vertical resistor R_d . This starts charging the channel film. The duration of the transient is set by τ_d . The initial jump is independent of τ_e .

The final value of the step current is

$$i_{df} = C_\mu \frac{\theta}{\beta_\mu \tau_e} \Delta V \quad (18)$$

This value gives the post-jump equilibrium current, hence $I_{df}^{st} = I_{d0}^{st} + i_{df}$.

2.3. The ac impedance model

To represent the small signal equations in the frequency domain, we make $d/dt \rightarrow s = i\omega$, where ω is the angular frequency and $i = \sqrt{-1}$. We have

$$i_g = \frac{1}{R_d} (v_g - v_h) \quad (19)$$

$$i_g = C_\mu s v_h \quad (20)$$

Combining Eqs. (19) and (20) we obtain

$$i_g = \frac{1}{Z_d} v_g \quad (21)$$

where the diffusion impedance is

$$Z_d = R_d + \frac{1}{C_\mu s} \quad (22)$$

The vertical impedance in Eq. (22) can be represented as an equivalent circuit shown in Fig. 1b.²⁸

The horizontal current is

$$I_d = -\theta \frac{qL}{\tau_e} A + C_{tv} \frac{du_h}{dt} \quad (23)$$

where

$$C_{tv} = f_B \beta_\mu C_\mu \quad (24)$$

The transversal capacitance C_{tv} in Eq. (24) is the chemical capacitance of holes in the channel. It is the same as the chemical capacitance of ions C_μ due to electroneutrality, but the factors in Eq. (24) indicate the part of the total chemical capacitance that contributes to the drain current.

The modulation of v_h induces a change of the drain current, according to the equation²⁸

$$i_d = \left(\frac{1}{R_{tv}} + C_{tv} s \right) v_h \quad (25)$$

where the transversal resistance

$$R_{tv} = \frac{\theta \beta_\mu \tau_e}{C_\mu} = \frac{\theta \beta_\mu L^2}{C_\mu \mu_p |u_{ds}|} \quad (26)$$

is associated to the modulation of the electronic carrier density by the gate voltage.

The effective relaxation time of the electronic channel is

$$R_{tv} C_{tv} = \theta f_B \beta_\mu^2 \tau_e = \theta \tau_h \quad (27)$$

where

$$\tau_h = f_B \beta_\mu^2 \tau_e \quad (28)$$

The transverse impedance v_g/i_d is represented as an equivalent circuit in Fig. 1c.²⁸

2.4. Standard expression of the current transient

The current transient in Eq. (13) can be expressed as

$$i_d(t) = i_{df} \left[1 - \left(1 - \theta \frac{\tau_h}{\tau_d} \right) e^{-t/\tau_d} \right] \quad (29)$$

In the case $\beta_\mu = \theta = 1$ we have

$$i_d(t) = i_{df} \left[1 - \left(1 - \frac{f_B \tau_e}{\tau_d} \right) e^{-t/\tau_d} \right] \quad (30)$$

This is the standard expression of the transient in BM model,^{15,20,24} but BM use an ionic time τ_i instead of the diffusion time τ_d . We will explain this difference in Section 3.3.

The linearized equations that are found in BM and in the above diffusion model provide significant insight to the physical components of the transient. However, for a large step of V_g the linear model cannot be used, and it is necessary to solve the nonlinear system formed by Eqs. (4, 5, 7). Based on this physical behaviour, if internal properties as the chemical capacitance and ions diffusion coefficient are very different at the initial and final point of the large voltage step, it is only natural that on and off switching times will be very different, as observed experimentally in “asymmetric” switching times.²⁵ This is a general property of transients in highly nonlinear systems: the apparent relaxation time is a function of the starting stationary point.³²

3. Model of transients with diffusion and interfacial/electrolyte impedances

3.1. The vertical current/voltage equations

To represent the electrolyte and interfacial limitations we add to the model of Fig. 1a the parallel combination of ionic resistance R_i and double layer capacitance C_d as shown in Fig. 3a, and we want to find a solution of the transient voltage and current for the extended system. The new vertical circuit is represented in the equivalent circuit of Fig. 3b. We remark that in an OCET model the C_d needs a parallel resistance, since the ionic current must penetrate the channel, and cannot be blocked at the interface.

The vertical current provides three equations²⁷

$$I_g = \frac{1}{R_i} (u_g - u_s) + C_d \frac{d(u_g - u_s)}{dt} \quad (31)$$

$$I_g = -\frac{qL}{\tau_d} [A(u_s) - A(u_h)] \quad (32)$$

$$I_g = C_\mu \frac{du_h}{dt} \quad (33)$$

Here, u_s is the voltage at the outer surface of the channel.

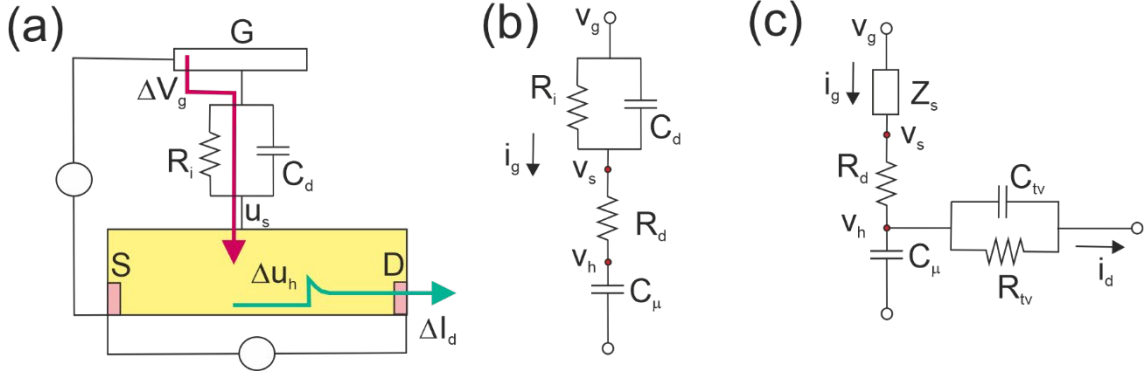


Fig. 3. (a) Scheme of the measurement of transient response of the OECT with series resistance and capacitor in the electrolyte. (b) The equivalent circuit for the vertical small signal ac impedance. (c) The equivalent circuit for the transversal impedance.

3.2. The transient of the vertical current

To solve for the time-dependent currents in Fig. 3a, we apply the same small perturbation method as in Sec. 2. We solve the response to an applied signal in the frequency domain. The solution in the time domain will be then obtained by inverse Laplace transform.

The vertical current equations become

$$i_g = \left(\frac{1}{R_i} + C_d s \right) (v_g - v_s) \quad (34)$$

$$i_g = \frac{1}{R_d} (v_s - v_h) \quad (35)$$

$$i_g = C_\mu v_h \quad (36)$$

We define the relaxation times

$$\tau_s = R_i C_d \quad (37)$$

$$\tau_{R\mu} = R_i C_\mu \quad (38)$$

The above equations yield the relation

$$v_h = \frac{1 + \tau_s s}{(1 + \tau_s s)(1 + \tau_d s) + \tau_{R\mu} s} v_g \quad (39)$$

Eq. (39) is the response of the internal voltage in the channel to the gate voltage perturbation.

Solving the quadratic equation in the denominator, and noting that $v_g = \Delta V/s$, we can write

$$v_h = \frac{1 + \tau_s s}{s(1 + \tau_1 s)(1 + \tau_2 s)} \Delta V \quad (40)$$

The fundamental relaxation times are

$$\tau_1 = 2 \frac{\tau_0}{1 - b} \quad (41)$$

$$\tau_2 = 2 \frac{\tau_0}{1+b} \quad (42)$$

where

$$\tau_0 = \left[\frac{1}{\tau_d} \left(1 + \frac{C_\mu}{C_d} \right) + \frac{1}{\tau_s} \right]^{-1} \quad (43)$$

$$b = \left(1 - 4 \frac{\tau_0^2}{\tau_d \tau_s} \right)^{1/2} \quad (44)$$

By inversion of (40) to the time domain we have the solution

$$v_h = \left[1 - (\delta_1 e^{-t/\tau_1} + \delta_2 e^{-t/\tau_2}) \right] \Delta V \quad (45)$$

$$\delta_1 = \frac{\tau_0}{b \tau_d} \left(\frac{\tau_1}{\tau_s} - 1 \right) \quad (46)$$

$$\delta_2 = \frac{\tau_0}{b \tau_d} \left(1 - \frac{\tau_2}{\tau_s} \right) \quad (47)$$

Eq. (45) is the relaxation of the internal voltage when a pulse $v_g = \Delta V$ is applied to the gate contact, that extends Eq. (13) to the more general situation. Note that $v_h(0) = 0$, $v_h(\infty) = \Delta V$. The $v_h(t)$ is not dependent on τ_e since there is no horizontal component of the perturbation. However, this simplification will change if τ_e is very long and influences the diffusion transport.²⁷

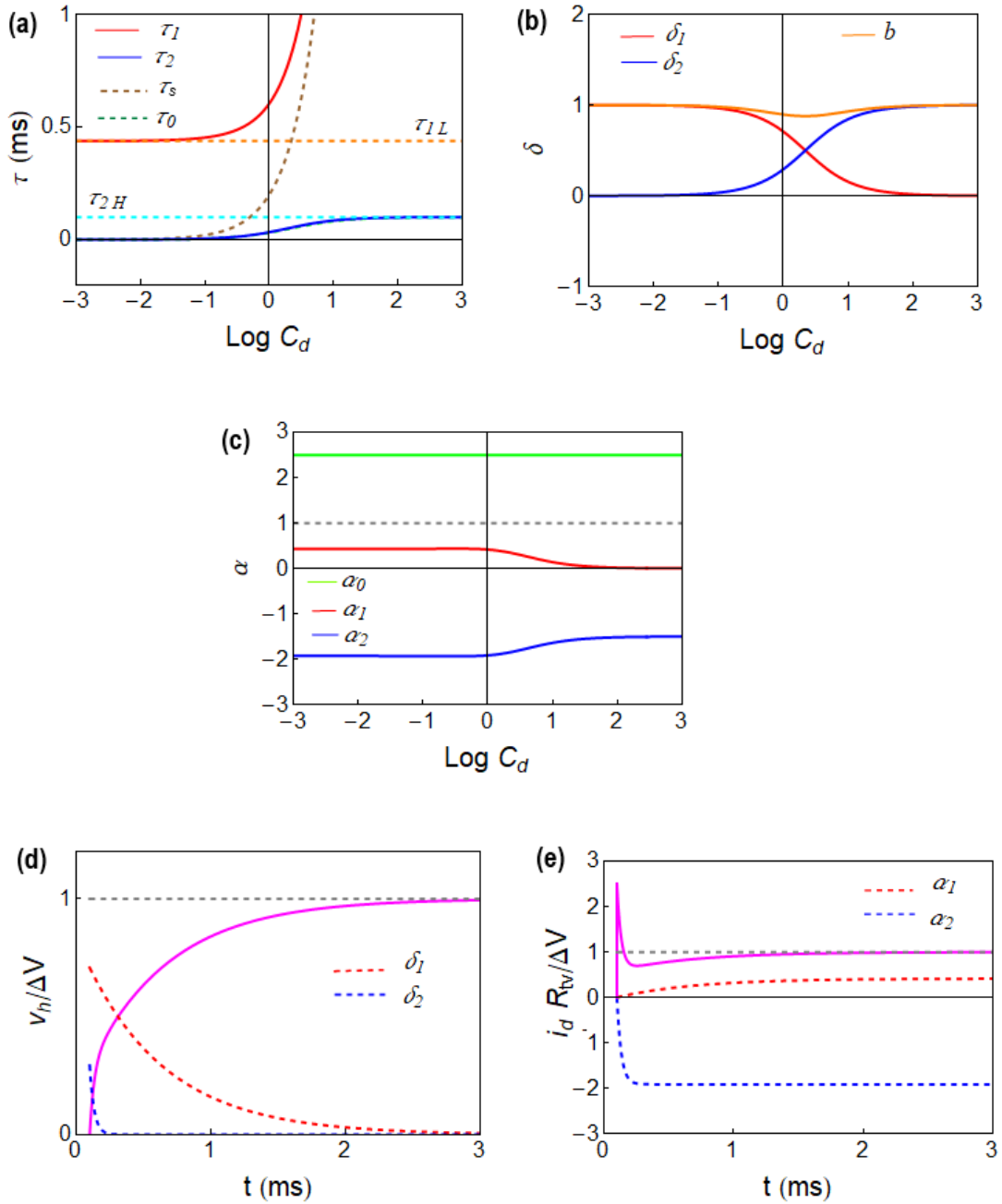


Fig. 4. (a) The relaxation times and (b, d) the weight factors of the transients. Parameters: $\tau_d = 0.1$, $\tau_e = 0.5$, $f_B = 0.5$, $R_i = 0.2$, $V_g = -0.5$, $C_\mu = 1.69$. (d, e) The transients of v_h and i_d for $C_d = 1$. The grey dashed line is the final equilibrium. Time in ms, V in V, R in $m\Omega$, C in F.

For the interpretation of these results, we turn to Fig. 4. The two fundamental decay time constants, τ_1 and τ_2 are plotted with respect to C_d in Fig. 4a, and the weights in the decay δ_i are shown in Fig. 4b. Note that $\tau_0 \approx \tau_2$ at all values of C_d . The voltage transient is shown in Fig. 4d, indicating the contribution of each component, for a particular value

of C_d .

Both τ_1 and τ_2 become independent of C_d at low and high C_d , respectively. To obtain the limiting values we first find the limits of τ_0 . For $C_d \ll C_\mu$ it is

$$\tau_{0L} = \left[\frac{1}{C_d R_d} + \frac{1}{\tau_s} \right]^{-1} \quad (48)$$

This is the charging of the surface capacitor C_d . While for $C_d \gg C_\mu$

$$\tau_{0H} = \left[\frac{1}{\tau_d} + \frac{1}{\tau_s} \right]^{-1} \quad (49)$$

Here is the charging of the surface capacitor limited by the charging of the chemical capacitance when C_d becomes large.

In Fig. 4b we note that for $C_d < C_\mu$ the decay is dominated by τ_1 , and it can be approximated as

$$\tau_{1L} = (R_i + R_d)C_\mu \quad (50)$$

For $C_d > C_\mu$, it is $\delta_1 \approx 0$ and $\delta_2 \approx 1$. Hence the second root dominates the decay for $C_d \gg C_\mu$, and it becomes

$$\tau_{2H} = \tau_{0H} = R_d C_\mu = \tau_d \quad (51)$$

Accordingly, we find that τ_2 corresponds to the original time constant τ_d in the diffusion model of Fig. 1 and 2, while τ_1 contains a contribution of the series resistance, Eq. (50), and it is always

$$\tau_{2H} < \tau_{1L} \quad (52)$$

and, more generally

$$\tau_2 < \tau_1 \quad (53)$$

Therefore, there are two components in the transient of v_h towards ΔV . τ_2 is the fast component and τ_1 the slow one, Fig. 4d. The diffusion charging (τ_2) happens first, and then occurs a slower charging due to the external resistor and capacitor (τ_1).

3.3. The transient of the horizontal current

We can write Eq. (25) as

$$i_d = \frac{1}{R_{el}} (1 + \theta \tau_h s) v_h \quad (54)$$

Therefore

$$i_d = \frac{\theta}{R_{el}} \frac{(1 + \tau_s s)(1 + \theta \tau_h s)}{(1 + \tau_1 s)(1 + \tau_2 s)} \frac{\Delta V}{s} \quad (55)$$

This model corresponds to Fig. 3c. The solution in the time domain is

$$i_d(t) = \left[\alpha_0 + \alpha_1 \left(1 - e^{-\frac{t}{\tau_1}} \right) + \alpha_2 \left(1 - e^{-\frac{t}{\tau_2}} \right) \right] \frac{\theta C_\mu}{\beta_\mu \tau_e} \Delta V \quad (56)$$

where

$$\alpha_0 = \frac{\theta \tau_s \tau_h}{\tau_1 \tau_2} \quad (57)$$

$$\alpha_1 = \frac{1}{(\tau_2 - \tau_1)} \left(-\tau_1 + \theta\tau_h + \tau_s - \frac{\theta\tau_h\tau_s}{\tau_1} \right) \quad (58)$$

$$\alpha_2 = \frac{1}{(\tau_2 - \tau_1)} \left(\tau_2 - \theta\tau_h - \tau_s + \frac{\theta\tau_h\tau_s}{\tau_2} \right) \quad (59)$$

We observe in Eq. (56) that the current transient contains two components governed by the fundamental time constants, τ_1 and τ_2 . The weights of the components are shown in Fig. 4c. The initial value of the current response is

$$i_{d,in} = \alpha_0 \frac{\Delta V}{R_{tv}} \quad (60)$$

and the final value is

$$i_{d,fin} = \frac{\Delta V}{R_{el}} \quad (61)$$

As commented before, τ_2 is the fast component, and this is observed in Fig. 4e, where the initial spike is the same as that in Fig. 2d, since $\tau_d < \tau_e$ in this example. But then the signal rises to a larger final value, due to the longer time constant τ_1 .

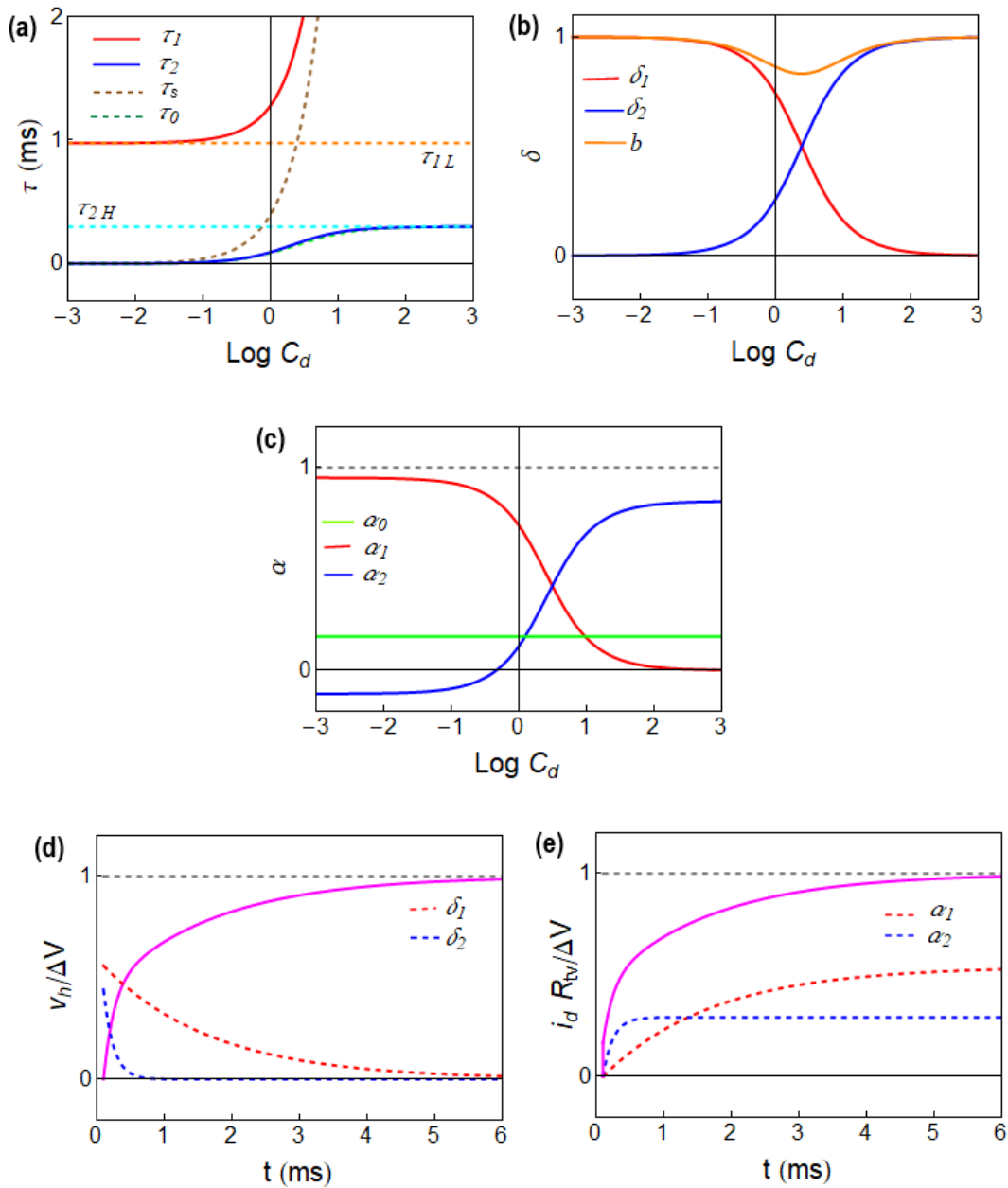


Fig. 5. (a) The relaxation times and (b, d) the weight factors of the transients. Parameters: $\tau_d = 0.3, \tau_e = 0.1, f_B = 0.5, R_i = 0.4, V_g = -0.5, C_\mu = 1.69$. (d, e) The transients of v_h and i_d for $C_d = 2$. The grey dashed line is the final equilibrium. Time in ms, V in V, R in $m\Omega$, C in F.

In Fig. 5 we show results for the opposite case in Fig. 2, $\tau_d > \tau_e$. In Fig. 5d we remark the rise of the voltage by the combination of the two fundamental time constants. In Fig. 5e we observe the components of the rise of the current: It starts at α_0 , shows a rapid rise by τ_2 , and a longer rise by τ_1 .

By Eq. (50) we can observe that

$$\tau_{1L} = R_i C_\mu \quad (62)$$

in the case in which the outer resistance is dominant. This is the time called τ_i in the Bernards-Malliaras model, where the transient is usually written as Eq. (31), with τ_i instead of the diffusion time τ_d . Note that BM model obtains a RC circuit similar to Fig. 1b but the resistance is interpreted as electrolyte transport.^{15,17} Instead, in Fig. 1b R_d and C_μ are associated to ion diffusion and accumulation inside the channel.²⁸

We arrive at the conclusion that BM expression is a particular case of Eq. (56), that contains both the external ionic resistance and diffusion inside the channel. Again, we remark that for a large transient step the full set of nonlinear equations must be solved to obtain the transient response.

4. Visualising the interface phenomena through 2D device modelling

The solubility difference is the most notable chemical-physics mechanism that defines the discontinuity associated with the interface between the solution and the semiconductor. This section aims to show how this would lead to an effective circuit of resistance in parallel to capacitance and that the resulting effect on the current transient agrees with the analytical model. We use the same simulation approach reported in refs. ^{23,27}, which consists of employing the Sentaurus device TCAD by Synopsys to solve ionic and electronic transport within a semiconductor device model framework. To our previous reports,^{23,27} we need to add the potential solubility difference at the solution/semiconductor interface with the ions being less soluble in the semiconductor. Henry's law for solubility³³ can be used to show that solubility difference dictates a concentration ratio between the two sides of the interface. Such a concentration (density) ratio corresponds to an energy barrier within a semiconductor device model framework. Hence, we will implement an energy barrier (E_b) that will enforce a density ratio of $\exp(-E_b/k_B T)$.

Fig. 6a shows the OECT device structure used in the simulations, and Table 2 lists the parameters implemented in the simulations. It is a P type OECT based on an undoped semiconductor where the penetration of anions from the solution would dope and switch it on. We show the hole density distribution inside the semiconductor for $V_{DS}=-0.1$ V, $V_{GS}=-0.05$ V, and $I_{DS}=10$ μ A (see red circle in Fig. 6b).

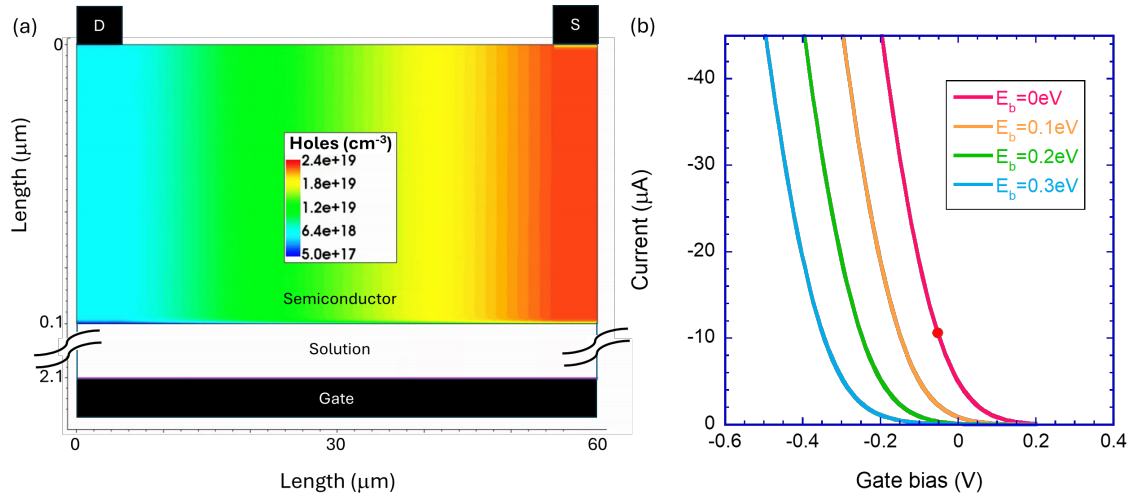


Fig. 6. (a) Schematic description of the OEET device structure exhibiting the hole density distribution for $V_{GS} = 0$ V, $V_{DS} = -0.1$ V, and no ionic injection barrier at the solution/semiconductor interface. (b) Current gate-voltage (output characteristics) of OEET devices for different ion injection barriers between the solution and the semiconductor. The lines show no-barrier (red line), 0.1 eV (orange line), 0.2 eV (green line), and 0.3 eV (cyan line). The red circle shows the point at which the densities in (a) were simulated. Note that the ion injection barrier shifts the curves (as a V_T shift).

Table 2. Device and material parameters used in the simulations

Device	Chanel length	50 μm
	Chanel width	50 μm
Semiconductor	Thickness	100 nm
	Hole mobility	5 cm^2/Vs
	Source-drain voltage	0.1 V
	Anion diffusivity	$10^{-8} \text{ cm}^2/\text{s}$
	Cation diffusivity	----
Solution	Anion diffusivity	$10^{-6} \text{ cm}^2/\text{s}$
	Cation diffusivity	$10^{-6} \text{ cm}^2/\text{s}$
	Salt concentration	10^{20} cm^{-3} (0.17 M)

In these simulations, the cations are insoluble in the semiconductor, and the anions injection barrier at the solution/semiconductor interface was implemented by enforcing a ratio of $\exp(-E_b/k_B T)$ between the anions on the semiconductor and solution sides of the interface. We first simulated the output characteristics of OEETs with different ionic injection barriers. Fig. 6b shows the output IV curves of OEETs having ionic injection barrier (E_b) of 0 eV (red line), 0.1 eV (orange line), 0.2 eV (green line), and 0.3 eV (cyan line). As expected, an injection barrier shifts the curve by the amount equivalent to the barrier energy converted to volts. (denoted $V_T = E_b/q$)

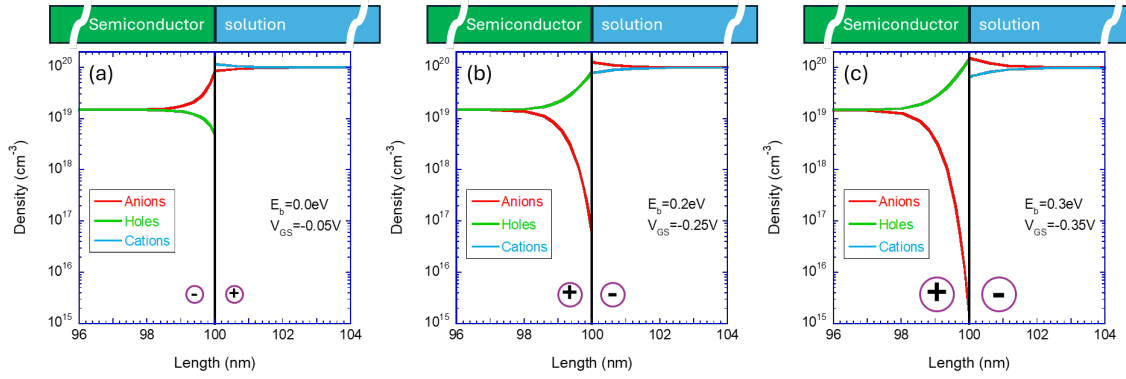


Fig. 7. Simulated charge carriers' density distribution close to the interface (black line) between the semiconductor (left) and the solution (right). The densities are along a cutline in the middle between the source and drain electrodes. The charge carriers are anions (red line), cations (cyan line), and holes (green line). (a) No ionic injection barrier ($E_b=0$), (b) $E_b=0.2\text{eV}$ (c) $E_b=0.3\text{eV}$. The circled + and – denote the net charge at the interface.

To understand the effect of the anions injection barrier on the interface properties, we plot in Fig. 7 the charge carriers' density distribution close to the interface (black line) between the semiconductor (left) and the solution (right). The charge carriers are anions (red line), cations (cyan line), and holes (green line). To place the devices with different injection barriers on equal footings, we chose gate voltages such that $(V_{GS} + V_T)$ is equal for the devices ($=50\text{ mV}$). Indeed, the hole and anion density in the bulk of the devices are identical ($1.5 \times 10^{19}\text{ cm}^{-3}$). The inherent discontinuity at the solution/semiconductor interface is expected to induce some polarization. Fig. 7a shows that without an ionic injection barrier, it extends about 1 nm from the interface. Considering Figures 7b and c, an ionic barrier produces a lower anion density on the semiconductor side, resulting in a higher injection resistance. Also, the ionic barrier induces hole and anion accumulation at the interface, possibly considered a double-layer capacitance. Between $E_b=0.2\text{eV}$ and $E_b=0.3\text{eV}$, the anion density at the interface is reduced by 30, and the integrated net charge close to the interface goes up by a factor of 1.7.

To simulate the transient response of the different devices, we applied a step to the gate bias, ensuring that the ON state corresponds to the same bias used for Fig. 7 ($V_{GS} + V_T = 50\text{mV}$). A barrier of 0.1eV had a negligible effect, and Fig. 8b shows the responses for ionic injection barrier (E_b) of 0eV (red line), 0.2eV (green line), and 0.3eV (cyan line). The longer time constant associated with a higher barrier aligns with our observation (Fig. 7) that the barrier induces a capacitance and a resistance. Based on our analysis of Fig. 7, the interface resistance is the dominant factor.

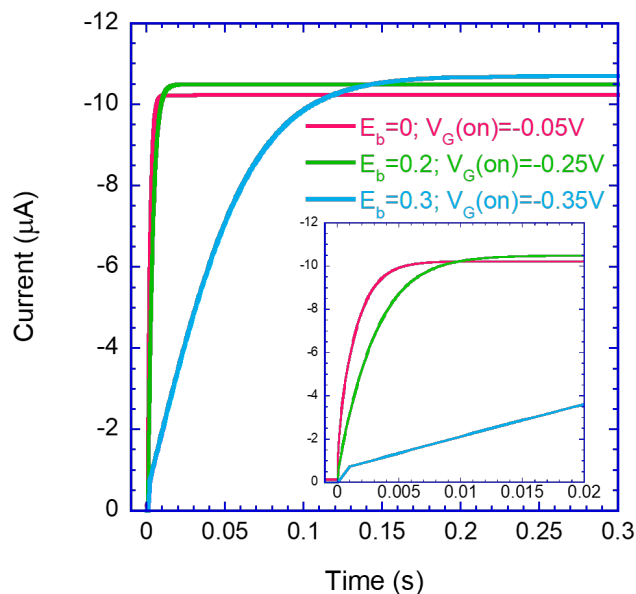


Fig. 8. Transient responses of the devices having different injection barriers following a gate voltage step from 0.2V to the voltage corresponding to $I_D=10\mu\text{A}$ (i.e., to the same V_G-V_T). $V_{DS}=-0.1\text{V}$. The inset is a zoom on the first 20 ms.

Conclusion

We established a general theory of the current transient of ionic-electronic transistors. The dominant effect when the gate voltage is changed is a transient charging of the channel by diffusion of ions. The additional influence of electrolyte capacitance and resistance splits the fundamental time constant of diffusion into two different components, τ_1 and τ_2 . The transient may become much larger than by diffusion alone by impediments of ion transport. The analysis of simulations enables to include more complete effects as the distribution of oppositely charged ions, but confirms the general trends obtained in the theory model. This method provides a convenient framework for the characterization of complex time domains responses of organic electrochemical transistors.

Acknowledgments

The work of Juan Bisquert was funded by the European Research Council (ERC) via Horizon Europe Advanced Grant, grant agreement n° 101097688 ("PeroSpiker"). This work was funded by the MCIN of Spain under project PID2022-141850OB-C21 Nir Tessler acknowledges the support by the Ministry of Innovation, Science and Technology Israel, the M-ERANET grant PHANTASTIC Call 2021.

Associated content

Data Availability Statement

The data presented here can be accessed at XXX (Zenodo) under the license CC-BY-4.0 (Creative Commons Attribution-ShareAlike 4.0 International).

References

- (1) Huang, M.; Schwacke, M.; Onen, M.; del Alamo, J.; Li, J.; Yildiz, B. Electrochemical Ionic Synapses: Progress and Perspectives, *Adv. Mater.* **2023**, *35*, 2205169.
- (2) Yao, X.; Klyukin, K.; Lu, W.; Onen, M.; Ryu, S.; Kim, D.; Emond, N.; Waluyo, I.; Hunt, A.; del Alamo, J. A.; Li, J.; Yildiz, B. Protonic solid-state electrochemical synapse for physical neural networks, *Nat. Commun.* **2020**, *11*, 3134.
- (3) Fuller, E. J.; Gabaly, F. E.; Léonard, F.; Agarwal, S.; Plimpton, S. J.; Jacobs-Gedrim, R. B.; James, C. D.; Marinella, M. J.; Talin, A. A. Li-Ion Synaptic Transistor for Low Power Analog Computing, *Adv. Mater.* **2017**, *29*, 1604310.
- (4) Nikam, R. D.; Kwak, M.; Lee, J.; Rajput, K. G.; Banerjee, W.; Hwang, H. Near ideal synaptic functionalities in Li ion synaptic transistor using Li3POxSex electrolyte with high ionic conductivity, *Sci. Rep.* **2019**, *9*, 18883.
- (5) Onen, M.; Emond, N.; Wang, B.; Zhang, D.; Ross, F. M.; Li, J.; Yildiz, B.; del Alamo, J. A. Nanosecond protonic programmable resistors for analog deep learning, *Science* **2022**, *377*, 539-543.
- (6) Harikesh, P. C.; Yang, C.-Y.; Wu, H.-Y.; Zhang, S.; Donahue, M. J.; Caravaca, A. S.; Huang, J.-D.; Olofsson, P. S.; Berggren, M.; Tu, D.; Fabiano, S. Ion-tunable antiambipolarity in mixed ion–electron conducting polymers enables biorealistic organic electrochemical neurons, *Nat. Mater.* **2023**, *22*, 242–248.
- (7) Matrone, G. M.; van Doremaele, E. R. W.; Surendran, A.; Laswick, Z.; Griggs, S.; Ye, G.; McCulloch, I.; Santoro, F.; Rivnay, J.; van de Burgt, Y. A modular organic neuromorphic spiking circuit for retina-inspired sensory coding and neurotransmitter-mediated neural pathways, *Nat. Commun.* **2024**, *15*, 2868.
- (8) Gkoupidenis, P.; Zhang, Y.; Kleemann, H.; Ling, H.; Santoro, F.; Fabiano, S.; Salleo, A.; van de Burgt, Y. Organic mixed conductors for bioinspired electronics, *Nat. rev. Mater.* **2024**, *9*, 134-149.
- (9) Paulsen, B. D.; Tybrandt, K.; Stavrinidou, E.; Rivnay, J. Organic mixed ionic–electronic conductors, *Nat. Mater.* **2020**, *19*, 13-26.
- (10) Keene, S. T.; Rao, A.; Malliaras, G. G. The relationship between ionic-electronic coupling and transport in organic mixed conductors, *Science Advances* **2023**, *9*, eadi3536.
- (11) Keene, S. T.; Laulainen, J. E. M.; Pandya, R.; Moser, M.; Schnedermann, C.; Midgley, P. A.; McCulloch, I.; Rao, A.; Malliaras, G. G. Hole-limited electrochemical doping in conjugated polymers, *Nat. Mater.* **2023**, *22*, 1121-1127.
- (12) Larsson, O.; Laiho, A.; Schmickler, W.; Berggren, M.; Crispin, X. Controlling the Dimensionality of Charge Transport in an Organic Electrochemical

Transistor by Capacitive Coupling, *Adv. Mater.* **2011**, *23*, 4764-4769.

(13) Lenz, J.; del Giudice, F.; Geisenhof, F. R.; Winterer, F.; Weitz, R. T. Vertical, electrolyte-gated organic transistors show continuous operation in the MA cm⁻² regime and artificial synaptic behaviour, *Nature Nanotechnology* **2019**, *14*, 579-585.

(14) Yamamoto, S.; Polyravas, A. G.; Han, S.; Malliaras, G. G. Correlation between Transient Response and Neuromorphic Behavior in Organic Electrochemical Transistors, *Adv. Electron. Mater.* **2022**, *8*, 2101186.

(15) Bernards, D. A.; Malliaras, G. G. Steady-State and Transient Behavior of Organic Electrochemical Transistors, *Adv. Func. Mater.* **2007**, *17*, 3538-3544.

(16) Rivnay, J.; Leleux, P.; Ferro, M.; Sessolo, M.; Williamson, A.; Koutsouras, D. A.; Khodagholy, D.; Ramuz, M.; Strakosas, X.; Owens, R. M.; Benar, C.; Badier, J.-M.; Bernard, C.; Malliaras, G. G. High-performance transistors for bioelectronics through tuning of channel thickness, *Science Advances* **2015**, *1*, e1400251.

(17) Friedlein, J. T.; Shaheen, S. E.; Malliaras, G. G.; McLeod, R. R. Optical Measurements Revealing Nonuniform Hole Mobility in Organic Electrochemical Transistors, *Advanced Electronic Materials* **2015**, *1*, 1500189.

(18) Friedlein, J. T.; Donahue, M. J.; Shaheen, S. E.; Malliaras, G. G.; McLeod, R. R. Microsecond Response in Organic Electrochemical Transistors: Exceeding the Ionic Speed Limit, *Adv. Mater.* **2016**, *28*, 8398-8404.

(19) Ohayon, D.; Druet, V.; Inal, S. A guide for the characterization of organic electrochemical transistors and channel materials, *Chemical Society Reviews* **2023**, *52*, 1001-1023.

(20) Faria, G. C.; Duong, D. T.; Salleo, A. On the transient response of organic electrochemical transistors, *Organic Electronics* **2017**, *45*, 215-221.

(21) Szymański, M. Z.; Tu, D.; Forchheimer, R. 2-D Drift-Diffusion Simulation of Organic Electrochemical Transistors, *IEEE Transactions on Electron Devices* **2017**, *64*, 5114-5120.

(22) Cea, C.; Zhao, Z.; Wisniewski, D. J.; Spyropoulos, G. D.; Polyravas, A.; Gelinas, J. N.; Khodagholy, D. Integrated internal ion-gated organic electrochemical transistors for stand-alone conformable bioelectronics, *Nat. Mater.* **2023**, *22*, 1227-1235.

(23) Bitton, S.; Tessler, N. Unveiling the Impact of the Electrolyte's Counter Ions on Organic Electrochemical Transistor Performance, *Advanced Electronic Materials* **2024**, 2300766.

(24) Zhao, C.; Lüssem, B.; Zhang, S.; Wang, S.; Ma, W. A universal pre-charging method for enhancing transient speed in Organic Electrochemical Transistors, *Giant* **2024**, *19*, 100306.

(25) Guo, J.; Chen, S. E.; Giridharagopal, R.; Bischak, C. G.; Onorato, J. W.;

Yan, K.; Shen, Z.; Li, C.-Z.; Luscombe, C. K.; Ginger, D. S. Understanding asymmetric switching times in accumulation mode organic electrochemical transistors, *Nat. Mater.* **2024**, *23*, 656-663.

(26) Zhao, C.; Lüssem, B.; Zhang, S.; Wang, S.; Ma, W. A Universal Pre-charging Method for Enhancing Transient Speed in Organic Electrochemical Transistors, *Giant* **2024**, 100306.

(27) Bisquert, J.; Ilyassov, B.; Tessler, N. Switching response in organic electrochemical transistors by ionic diffusion and electronic transport *Advanced Science* **2024**, 2404182.

(28) Bisquert, J.; Keene, S. T. Ionic-electronic transistors small signal AC admittance: Theory and experiment, **2024**, <http://arxiv.org/abs/2408.02648>.

(29) Paulsen, B. D.; Frisbie, C. D. Dependence of Conductivity on Charge Density and Electrochemical Potential in Polymer Semiconductors Gated with Ionic Liquids, *J. Phys. Chem. C* **2012**, *116*, 3132-3141.

(30) Zhang, F.; Dai, X.; Zhu, W.; Chung, H.; Diao, Y. Large Modulation of Charge Carrier Mobility in Doped Nanoporous Organic Transistors, *Adv. Mater.* **2017**, *29*, 1700411.

(31) Janssen, M.; Bisquert, J. Locating the frequency of turnover in the thin-film diffusion impedance, *J. Phys. Chem. C* **2021**.

(32) Bisquert, J. Hysteresis, Rectification and Relaxation Times of Nanofluidic Pores for Neuromorphic Circuit Applications, *Advanced Physics Research* **2024**, *3*, 2400029.

(33) Nicollian, E. H.; Brews, J. R. *MOS (Metal Oxide Semiconductor) Physics and Technology*; Wiley, 2022.